

CONSTRAINING A MODEL OF TURBULENT CORONAL HEATING FOR AU MICROSCOPII WITH X-RAY, RADIO, AND MILLIMETER OBSERVATIONS

STEVEN R. CRANMER, DAVID J. WILNER, AND MEREDITH A. MACGREGOR
 Harvard-Smithsonian Center for Astrophysics, 60 Garden Street, Cambridge, MA 02138, USA

Draft version September 4, 2018

ABSTRACT

Many low-mass pre-main-sequence stars exhibit strong magnetic activity and coronal X-ray emission. Even after the primordial accretion disk has been cleared out, the star’s high-energy radiation continues to affect the formation and evolution of dust, planetesimals, and large planets. Young stars with debris disks are thus ideal environments for studying the earliest stages of non-accretion-driven coronae. In this paper we simulate the corona of AU Mic, a nearby active M dwarf with an edge-on debris disk. We apply a self-consistent model of coronal loop heating that was derived from numerical simulations of solar field-line tangling and magnetohydrodynamic turbulence. We also synthesize the modeled star’s X-ray luminosity and thermal radio/millimeter continuum emission. A realistic set of parameter choices for AU Mic produces simulated observations that agree with all existing measurements and upper limits. This coronal model thus represents an alternative explanation for a recently discovered ALMA central emission peak that was suggested to be the result of an inner “asteroid belt” within 3 AU of the star. However, it is also possible that the central 1.3 mm peak is caused by a combination of active coronal emission and a bright inner source of dusty debris. Additional observations of this source’s spatial extent and spectral energy distribution at millimeter and radio wavelengths will better constrain the relative contributions of the proposed mechanisms.

Keywords: radio continuum: stars – stars: coronae – stars: individual (AU Microscopii) – submillimeter: stars – turbulence – X-rays: stars

1. INTRODUCTION

Nearly all low-mass stars are believed to have magnetic fields that influence their surroundings and evolution. Young stars with ages less than 10–20 Myr exhibit high-energy activity in the form of hot coronal loops, flares, accretion shocks, and open-field regions with winds or jet-like outflows (see, e.g., Feigelson & Montmerle 1999; McKee & Ostriker 2007; Güdel & Nazé 2009; Günther 2013). Because the magnetic fields of the star and disk are threaded together with one another, it is often difficult to disentangle the contributions from various proposed sources of activity. On the other hand, the situation may be greatly simplified for older stars that have evolved past the classical T Tauri phase. These stars have lost their dense gas disks, and thus the major remaining contributor to the star’s ultraviolet and X-ray emission is the presence of magnetic coronal loops. In that case, the subsequent evolution of a star’s *coronal heating* as it starts main sequence hydrogen burning may no longer involve drastic changes in the source regions, but instead just be the result of a gradual evolution in parameters related to its magnetohydrodynamic (MHD) dynamo (Hartmann & Noyes 1987; Wright et al. 2011; Stelzer et al. 2013).

Pre-main-sequence stars with debris disks are ideal targets for studying the earliest stages of non-accretion-driven magnetic activity. In this paper we focus on AU Microscopii (HD 197481, GJ 803), a nearby M1Ve flare star with a well-resolved debris disk. Having an effective temperature of ~ 3500 K, AU Mic probably is not fully convective like the later-type M dwarfs. Thus, its MHD dynamo may be qualitatively similar to those of more massive stars like the Sun. AU Mic is bright in X-rays (Schneider & Schmitt 2010), rich in ultraviolet flaring phenomena (Robinson et al. 2001), and surrounded by an edge-on dust disk with a mass of roughly $1 M_{\text{Moon}}$ and a spatial extent similar to the Kuiper belt

in our solar system (e.g., Kalas et al. 2004; Liu et al. 2004; Augereau & Beust 2006; Wilner et al. 2012).

Recently, MacGregor et al. (2013) observed AU Mic at millimeter wavelengths with the Atacama Large Millimeter/submillimeter Array (ALMA). In addition to the Kuiper-like dust belt, they were able to distinguish a compact central emission peak with a flux of $\sim 320 \mu\text{Jy}$. The origin of this component is not yet known. The M dwarf’s stellar photosphere would generate a blackbody flux of only about $60 \mu\text{Jy}$ at $\lambda = 1.3$ mm, a factor of 5 smaller than the observed emission peak. In order for a star-sized blackbody to be responsible for the observed emission, it would need to have a temperature of roughly 17,000 K. This kind of dominant chromospheric emission was predicted by Harper et al. (2013) for cool evolved giants, but those stars have much larger emitting areas and no significant coronal emission. An M dwarf like AU Mic may have a thin chromosphere underneath its hot corona, but its optical depth is not likely to be high enough to generate a photosphere-like blackbody spectrum.

MacGregor et al. (2013) suggested that the central emission peak of AU Mic may be produced by an inner “asteroid belt” of cool dust grains or planetesimals within ~ 3 AU of the star. Only about $0.01 M_{\text{Moon}}$ worth of dust material needs to be present to generate the observed emission peak; this is comparable to the mass of the asteroid belt in our solar system. MacGregor et al. (2013) also computed upper limits on the required temperatures of silicate grains in this proposed belt and found values of 35–75 K. This range is the same order of magnitude as the expected dust temperatures at a distance of $\lesssim 3$ AU from an M dwarf.

In this paper we propose an alternate explanation for the ALMA central emission component of AU Mic. Since this star has such strong X-ray emission, we explored the possibility that a collection of *hot coronal loops* on its surface could be responsible for similarly strong thermal emission at

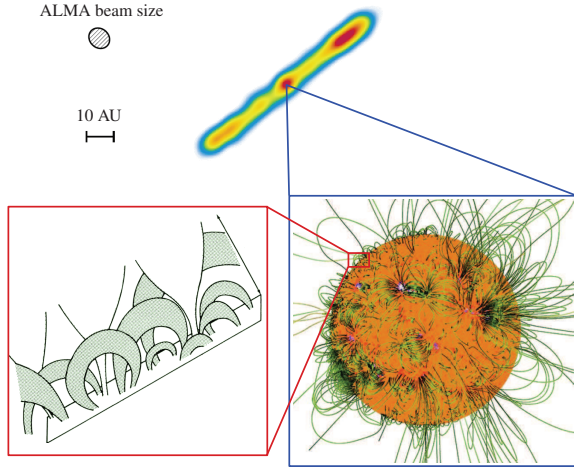


Figure 1. Proposed scenario for coronal emission from AU Mic. Clockwise from top: ALMA 1.3 mm continuum emission map (adapted from MacGregor et al. 2013); example potential field reconstruction of the solar magnetic field (Wiegmann & Sakurai 2012); schematic illustration of open and closed magnetic regions in the low corona (Dowdy et al. 1986).

1.3 mm. Figure 1 illustrates the suggested MHD circumstellar environment, where magnetic loops with a continuous distribution of sizes are assumed to fill the corona with $\sim 10^6$ K plasma. We aim to create a single model of these loops that reproduces the available observations at X-ray and millimeter wavelengths. White et al. (1994) also explored the use of radio continuum measurements as constraints to models of M dwarf coronal heating. In a way, this paper follows on from the general ideas described by White et al. (1994), but our models are based on self-consistent physical sources of plasma heating inspired by recent advances in understanding the Sun’s well-resolved corona.

In Section 2 of this paper, we describe the model of coronal heating that we apply to AU Mic. Section 3 summarizes how we synthesize observable quantities in the X-ray, radio, and millimeter wavelength bands for later comparison with observations. In Section 4 we present the computed coronal loop parameters for AU Mic as well as synthetic X-ray luminosities and radio/mm spectra. Section 5 concludes the paper with a brief summary of the main results and suggestions for future improvements.

2. CORONAL HEATING MODEL

In this section we describe a model of turbulence-driven coronal activity motivated by the present-day Sun. The model adopts a time-steady description of coronal heating and does not attempt to simulate the full range of intermittent and chaotic MHD dynamics that is evident in high-resolution solar images (e.g., Cirtain et al. 2013). Nonetheless, such a phenomenological description of turbulence has been shown to accurately reproduce many properties of coronal heating and wind acceleration for the Sun (Cranmer 2012). Also, Cranmer (2009) showed how this model performs well in predicting the X-ray activity of young stars undergoing active accretion, and Cranmer & Saar (2011) used the model to compute the mass-loss rates of stellar winds for stars with a wide range of ages and masses.

The basic idea is that magnetic field lines at the stellar photosphere are continually jostled by a stochastic source of mechanical energy, and this gives rise to MHD waves that prop-

agate up to larger heights and eventually dissipate. In tandem with wave generation, the random footpoint motions produce an increase in the overall magnetic energy via the twisting, shear, and braiding of field lines (e.g., Parker 1972). The transport and dissipation of magnetic energy from both waves and braiding can be described using the unifying language of *turbulent cascade* (van Ballegoijen 1986; Gómez et al. 2000; Rappazzo et al. 2008; van Ballegoijen et al. 2011). The presence of radiative cooling in such a system produces a thermal instability that often leads to the coexistence of a cool ($T \lesssim 10^4$ K) chromosphere and a hot ($T \gtrsim 10^6$ K) corona. In the ionized corona, heat conduction also makes for a “thermostat” effect in which the time-steady spatial distribution of T is much smoother than the spatial distribution of the heating rate.

There are several possible sources of stochastic mechanical energy at the photospheric base. Convective granulation surely plays a major role for most low-mass stars (Musielak 2004). For stars undergoing active accretion, an additional source of energy can exist in the form of ripples from the impact of gas clumps falling down from above (Cranmer 2008). It has also been suggested that the presence of planets in a magnetized stellar wind may give rise to MHD fluctuations that propagate back down to the star (e.g., Lanza 2012). For the purposes of this paper, we will treat the total available mechanical energy flux at the photosphere as a free parameter.

We describe the star itself by its fundamental parameters (mass, radius, luminosity, and metallicity) and ignore rotation. The dynamics of the jostled magnetic flux tubes are described by three additional parameters defined at the photosphere: mass density ρ_* , magnetic field strength B_* , and the mean energy flux F_A of Alfvén waves that propagate upwards as a result of the stochastic motion. To compute the density as a function of effective temperature T_{eff} and gravity g , we used the standard criterion that the Rosseland mean optical depth τ_R should have a value of $2/3$ in the photosphere, which demands

$$\tau_R \approx \kappa_R \rho_* H_* = 2/3. \quad (1)$$

The Rosseland mean opacity κ_R was interpolated from tables given by Ferguson et al. (2005), and we defined the density scale height in the photosphere as

$$H_* = \frac{k_B T_{\text{eff}}}{\mu m_H g}, \quad (2)$$

where k_B is Boltzmann’s constant and m_H is the mass of a hydrogen atom. Cranmer & Saar (2011) found that, for cool-star photospheres, the mean atomic weight μ is a relatively slowly varying function of T_{eff} ; we used their parameterization.

To specify the photospheric magnetic field strength, we assumed that B_* remains linearly proportional to the so-called equipartition field strength (i.e., the value at which magnetic pressure balances gas pressure). We used the proportionality constant found from observations by Cranmer & Saar (2011) to specify

$$B_* = 1.13 \sqrt{\frac{8\pi \rho_* k_B T_{\text{eff}}}{\mu m_H}} \quad (3)$$

for the footpoints of coronal loops. The Alfvén wave energy flux can be written in terms of the surface velocity amplitude v_\perp of transverse MHD waves, with $F_A = \rho_* v_\perp^2 V_A$, and the Alfvén speed is given by $V_A = B_*/\sqrt{4\pi\rho_*}$. We can make an initial estimate of the expected velocity amplitude using

turbulent convection models. Cranmer & Saar (2011) used the models of Musielak & Ulmschneider (2002) for main sequence and evolved stars. We find below, however, that for AU Mic the Musielak & Ulmschneider (2002) models predict an amplitude that is far too small to explain its observed coronal heating and X-ray activity. (Our understanding of the magnetic dynamos of young, rapidly rotating stars is still incomplete; see Section 5.)

In general, we assume that magnetic flux tubes fill only a fraction f_* of the stellar photosphere, so that the mean magnetic flux density of the star would be given by $\langle B \rangle \approx f_* B_*$. For the Sun, f_* varies between about 10^{-3} and 10^{-1} over location and activity cycle (Schrijver & Harvey 1989). The local magnetic field strength $B(r)$ inside a flux tube drops rapidly from B_* to $\langle B \rangle$ as a function of increasing height. However, for young stars in the “saturated” part of the age–activity–rotation diagram, Saar (2001) and Cranmer & Saar (2011) found that $f_* = 1$ is not a bad approximation to make. We will assume this for AU Mic as well (see additional discussion in Section 4), and this also allows us to assume that B_* remains constant over each coronal loop.

We note that f_* describes the filling factor of all magnetic flux tubes, of both polarities, that pass through the stellar surface. By itself, our assumption of $f_* = 1$ does not directly imply a prediction for the fraction of the magnetic field lines that are open (presumably to the stellar wind) versus those that are closed. The open/closed fraction depends on both the overall level of gas pressure in the stellar wind and the spatial patterns of imbalance between flux tubes with positive and negative polarities (Close et al. 2003; Cranmer & van Ballegooyen 2010). Below, we do assume the entire surface is covered by loops of varying lengths, but the coronal heating—and thus the X-ray and radio/mm emission—from the longest loops is likely to be not too different from the emission from open-field regions (see, e.g., Schrijver et al. 2004).

To specify the rate of plasma heating, we use a general expression for the rate of energy flux in the cascade from large to small eddies that was derived from analytic and numerical studies of MHD turbulence. Following Cranmer (2009), we define the heating rate (in units of power generated per unit volume) as

$$Q = \frac{\rho v_\perp^3}{\lambda_\perp} \left(\frac{\lambda_\perp V_A}{v_\perp L} \right)^\alpha, \quad \text{where } \alpha = \frac{2+420\mathcal{R}}{1+280\mathcal{R}} \quad (4)$$

and $\mathcal{R} = v_\perp/V_A$. The quantity λ_\perp is a transverse correlation length for the largest driving eddies, and is typically found to be of the same order of magnitude as the radius of the flux tube (e.g., Hollweg 1986). By convention, L is the half-length of the coronal loop. Nonzero values of the exponent α describe departures from an ideal Kolmogorov (1941) hydrodynamic cascade; such departures occur because of the specific MHD nature of wave-packet collisions that comprise the eddies in the presence of a strong background field. In closed loops, α can vary between 1.5 and 2. Our expression for the dependence of α on the wave amplitude v_\perp and Alfvén speed V_A was derived from the models of Rappazzo et al. (2008).

Even though Equation (4) utilizes constant values for v_\perp , λ_\perp , L , and B_* (in the definition of V_A), the density ρ is known to decrease rapidly as a function of height in a stellar atmosphere. Thus, because $V_A \propto \rho^{-1/2}$, the heating rate itself varies with density as $Q \propto \rho^{1-(\alpha/2)}$. For $\alpha = 2$ the heating rate is constant (as was assumed by Rosner et al. 1978), and for $\alpha < 2$

the heating is stronger at the high-density footpoints. The values of ρ and V_A at the “coronal base” (i.e., just above the sharp transition region between chromosphere and corona) are not the same as the corresponding values in the photosphere; these quantities are computed self-consistently by the model and are not specified as inputs.

In order to determine the time-steady coronal response to a given heating rate Q , we must consider how the injected heat is transported along the field by conduction and lost by radiation. We use the energy balance model of Martens (2010) to solve for the temperature T and electron number density n_e as a function of distance along a given loop of half-length L (see also Rosner et al. 1978; Aschwanden & Schrijver 2002). These quantities are specified by first computing the peak temperature T_{\max} at the top of the loop and the base pressure P . Martens (2010) parameterized the heating rate as $Q = hT^a P^b$, where h and P are assumed to be constants as a function of distance. For the heating model of Equation (4), the exponents are given by $a = -b = (\alpha/2) - 1$. Martens (2010) derived two scaling laws that allow one to solve for any two of the four loop quantities (L , T_{\max} , P , h) if the other two are provided. In our case, these scaling laws are given by

$$T_{\max} \propto h^{2/(2\alpha+3)} L^{(2+\alpha)/(2\alpha+3)}, \quad P \propto T_{\max}^3 / L, \quad (5)$$

and the unspecified constants of proportionality are described in detail by Martens (2010). These constants depend on the exponent α , the heat conductivity coefficient $\kappa = 1.1 \times 10^{-6}$ erg cm $^{-1}$ s $^{-1}$ K $^{-7/2}$, and the assumed properties of radiative cooling. For the latter, we assumed $Q_{\text{cool}} = \chi P^2 T^{-2.5}$, with a value of $\chi = 3.65 \times 10^{12}$ cm 4 s $^{-1}$ K $^{3/2}$, which we enhanced slightly over the solar value because of the higher metallicity of AU Mic (see Equation 21 of Cranmer & Saar 2011).

In order to model the thermal state of a given loop with half-length L , we use Equation (4) to determine h in terms of the other input parameters, and we use the scaling laws given in Equation (5) to solve for T_{\max} and P . The density at the coronal base is determined mainly by P , but it needs to be specified initially in order to compute V_A and α in Equation (4). Thus, we solve for these quantities iteratively by starting with the initial guess that the density is given by ρ_* . Cycling back through the equations gives rise to a converged and self-consistent value of ρ (and thus also V_A and α) typically within 10–15 iterations, and we run it for a total of 50 iterations to ensure accuracy. This converged value of the coronal base density is often 3–6 orders of magnitude smaller than ρ_* , which produces typical basal n_e values of 10^{10} – 10^{14} cm $^{-3}$.

Once T_{\max} and P are known for a given loop, we solved for the spatial dependence of temperature and density along the loop length s . Martens (2010) found that the temperature dependence $T(s)$ can be written as the inverse of an incomplete beta function; we used Equation (25) of Martens (2010) to obtain $T(s)$, and then we combined it with the ideal gas equation of state to solve for $n_e(s)$ as a function of P and $T(s)$. The minimum value of T at the coronal base was fixed at 10^4 K.

Lastly, we must take account of the fact that there should be a continuous distribution of loop lengths L across the surface of the star. We specify a normalized probability distribution $N(L)$ that describes the chances of finding a loop at any given value of L at a random location on the star. The shape of $N(L)$ depends on many details about the strength and topology of the magnetic field. The large-scale magnetic geometry of M dwarfs is beginning to be understood observationally (e.g., Gastine et al. 2013), but we know from the Sun

that the X-ray and UV emission is dominated by activity on spatial scales much smaller than have been resolved so far on other stars. Thus, we follow Cranmer (2009) and assume a power-law probability distribution, $N(L) \propto L^{-\varepsilon}$, with sharp cutoffs below minimum and maximum loop lengths L_{\min} and L_{\max} . The exponent ε in the loop-length distribution is another key free parameter of this model. The shortest loops are defined geometrically as those for which the central hole in the torus shrinks to zero; i.e., $L_{\min} = \pi r_{\perp}/2$, where r_{\perp} is the modeled poloidal radius of the loop (see Section 4). The longest loops are assumed to have lengths of order the stellar radius. We note that some young stars may have loops that extend out to even larger heights (Jardine & van Ballegoijen 2005; Aarnio et al. 2012). Nonetheless, it is not known what fraction of the very longest loops remain stable and closed in the presence of a stellar wind. Thus, we set $L_{\max} = R_*$ and assume that the coronal emission is relatively insensitive to the details of what happens for the small fraction of the star covered by the longest loops.

3. SYNTHESIS OF X-RAY AND RADIO/MILLIMETER EMISSION

To simulate a full distribution of loops covering the surface of AU Mic, we constructed 100 coronal models on a logarithmic grid in L that spans the ~ 3.5 orders of magnitude between L_{\min} and L_{\max} . We synthesized the observable quantities described below for the 100 models individually—assuming for each that the star is filled with loops of a given length—then we convolved them together using $N(L)$ to produce a result that is weighted properly over the statistical distribution of loop sizes.

We computed the total X-ray luminosity L_X under the optically thin assumption that all radiation escapes from the emitting regions. To maintain continuity with past observations of cool-star X-rays, we chose to use the response function of the *ROSAT* Position Sensitive Proportional Counter (PSPC) given by Judge et al. (2003). This function has nonzero sensitivity between about 0.1 and 2.4 keV, with a minimum around 0.3 keV that separates the hard and soft bands. Cranmer (2009) presented the temperature-dependent radiative loss rate $\Lambda_X(T)$ that is consistent with this response function, which is then used to estimate the X-ray luminosity,

$$L_X = 4\pi R_*^2 \int dz [n_e(z)^2] \Lambda_X[T(z)]. \quad (6)$$

We integrated down through the length of each loop, from $z = L$ to $z = 0$, under the simplifying geometric assumption that the loop is oriented vertically. In other words, we assumed that each loop has been “snipped in two” and the two ends are pointing radially upward. We also ignored foreshortening effects that would alter the path lengths through loops close to the stellar limb.

Calculating the emission at radio and millimeter wavelengths was slightly more complicated than the X-ray luminosity because we can no longer assume an optically thin emitting region. Thus, we solved the diffuse term in the formal solution to the equation of radiative transfer by integrating both the optical depth τ_ν and the specific intensity I_ν simultaneously, with

$$I_\nu = \int dz \chi_\nu \frac{2k_B T \nu^2}{c^2} e^{-\tau_\nu} \quad (7)$$

$$\tau_\nu = \int dz \chi_\nu \quad (8)$$

and we made the standard assumption that the source function is given by the Rayleigh-Jeans tail of the local Planck function. Because the plasma conditions vary rapidly as a function of position z along the loop, we did *not* make the other standard assumption that the source function is constant over the emitting area. As above, we integrated down from $z = L$ to $z = 0$, so that the resulting optical depth increases as z decreases.

For wavelengths λ between 0.01 and 100 cm, we assumed the radiation is dominated by thermal free-free emission (bremsstrahlung) and that the opacity is given by

$$\chi_\nu = 0.01 n_e^2 T^{-3/2} \nu^{-2} \ln \left(\frac{4.7 \times 10^{10} T}{\nu} \right) \quad (9)$$

in cgs units (see Dulk 1985; Güdel 2002). For the Gaunt factor (i.e., the natural logarithm term above), we used a fully ionized approximation that should apply for $T \gtrsim 3 \times 10^5$ K. Equation (9) also assumes $\nu \gg \nu_p$, where ν_p is plasma frequency in Hz; this condition is satisfied easily for the ALMA submillimeter wavelengths of interest and is satisfied marginally for longer radio wavelengths. For a star at distance D , we converted the surface-averaged specific intensity I_ν to flux S_ν by assuming that short loops (with $L \ll R_*$) generally dominate the emission and that there is no limb brightening or limb darkening. Thus, we used $S_\nu = \pi R_*^2 I_\nu / D^2$.

4. RESULTS FOR AU MIC

Table 1 gives the basic stellar parameters that we used either as inputs (upper part) or as after-the-fact constraints (lower part) on the models. The photospheric density ρ_* and magnetic field strength B_* were computed using the equations discussed above. The photospheric turbulence length scale λ_{\perp} and flux tube radius r_{\perp} were scaled down from canonical solar values of 300 km and 200 km, respectively, by the ratio of photospheric scale heights. The solar value of λ_{\perp} comes from models of Alfvén wave damping in the fast solar wind (Cranmer & van Ballegoijen 2005) and r_{\perp} comes from measurements of magnetic bright points (Berger et al. 1995, 2007); both are related closely to the horizontal sizes of magnetic features sitting between the granulation cells. Recent convection models (e.g., Robinson et al. 2004; Magic et al. 2013) show that the diameters of granules remain linearly proportional to the vertical scale height H_* over a wide range of stellar parameters.¹ We assume that intergranular features like magnetic flux tubes scale with H_* similarly as the cells. With the values given above, we found that the coronal loops of AU Mic span about 3.5 orders of magnitude in length between $L_{\min} = 190$ km and $L_{\max} = 5.83 \times 10^5$ km.

For AU Mic, we assumed the photospheric magnetic filling factor f_* is equal to 1. AU Mic appears to be safely inside the “saturated” regime of stellar activity that is consistent with this assumption. Its rotation period $P_{\text{rot}} \approx 4.8$ days implies a dimensionless Rossby number (i.e., P_{rot}/τ_c , where τ_c is the convective turnover time) of 0.05–0.1 (Hebb et al. 2007). Figure 7(b) of Cranmer & Saar (2011) shows $f_* \approx 1$ for a large sample of cool stars in this range of Rossby number. AU Mic also has an X-ray luminosity ratio L_X/L_{bol} of 0.0015, which is in the saturated part of the empirical age–activity–rotation diagram (e.g., Wright et al. 2011). Testa et al. (2004) estimated

¹ Note, however, that rotation is *not* one of the stellar parameters varied in most stellar convection simulations. See Section 5 for additional discussion of how rapid rotation may invalidate some traditional ideas about convection and magnetic activity.

Table 1
AU Mic Stellar Parameters

Distance	9.91 pc	van Leeuwen (2007)
M_*	$0.5 M_\odot$	Strubbe & Chiang (2006)
R_*	$0.838 R_\odot$	Houdebine (2009)
T_{eff}	3493 K	Houdebine (2009)
[Fe/H]	0.154	Houdebine (2009)
ρ_*	$9.2 \times 10^{-7} \text{ g cm}^{-3}$	Equation (1)
B_*	2200 G	Equation (3)
λ_\perp	182 km	see text
r_\perp	121 km	see text
L_X	$5.549 \times 10^{29} \text{ erg s}^{-1}$	Hünsch et al. (1999)
S_ν ($\lambda = 1.3 \text{ mm}$)	$320 \pm 60 \mu\text{Jy}$	MacGregor et al. (2013) ^a
S_ν ($\lambda = 2.0 \text{ cm}$)	$< 210 \mu\text{Jy}$	White et al. (1994)
S_ν ($\lambda = 3.7 \text{ cm}$)	$< 120 \mu\text{Jy}$	White et al. (1994)

^a AU Mic was observed by ALMA with its Band 6 receivers over four 2 hr long scheduling blocks between 2012 April 23 and 2012 June 16. These data are designated ADS/JAO.ALMA#2011.0.00142.S.

the filling factor of “solar-like active region” plasma in the corona of AU Mic to be roughly 0.9–1. Although this measurement does not constrain the *photospheric* value of f_* , it helps to show that the coronal flux tubes eventually fill the entire circumstellar volume.

The one remaining major parameter that is not yet determined for AU Mic is the surface flux of Alfvén waves. Cranmer & Saar (2011) used the models of Musielak & Ulmschneider (2002) to produce a fitting formula that gives this surface flux as a function of a star’s T_{eff} and $\log g$. For the parameters of AU Mic this formula gives $F_A \approx 2 \times 10^6 \text{ erg cm}^{-2} \text{ s}^{-1}$, which is equivalent to $v_\perp \approx 0.02 \text{ km s}^{-1}$. On the other hand, both observations of microturbulent broadening (Giampapa et al. 1982) and three-dimensional convection simulations (Wende et al. 2009; Beeck et al. 2011) show vigorous overturning motions with velocities of order 1–2 km s^{−1} for M dwarfs. For the Sun, the granulation velocities and surface wave amplitudes are roughly of the same order of magnitude as one another, but we do not know if this holds true for M dwarfs. Thus, we treat v_\perp as a free parameter, but we also note that values of order 1–2 km s^{−1} may be the most realistic.

We computed models of coronal heating for a grid of loops having lengths L between 10^2 and 10^6 km, and footpoint wave amplitudes v_\perp between 0.02 and 200 km s^{−1}. Figure 2 shows the resulting dependence of T_{max} and P on these two parameters. Each of these models had its own iterated value of the α exponent, and the largest values ($\alpha \approx 2$) tended to occur for the lowest velocity amplitudes and the longest loops; the smallest values ($\alpha \approx 1.5$) occurred for the largest amplitudes and shortest loops. The overall dependence of T_{max} and P on the two varied parameters is close to what is expected from the scaling laws given in Section 2. For example, if we use the average value of $\alpha = 1.78$ for this set of models, the scaling laws give

$$T_{\text{max}} \propto v_\perp^{0.37} L^{0.034}, \quad P \propto v_\perp^{1.12} L^{-0.90} \quad (10)$$

which agrees well with the plotted results. The curves shown in Figure 2 are not exact power laws because α itself is not constant.

In order to begin the process of testing our coronal models against real observations of AU Mic, we assembled together the temperature and density distributions for individual loop lengths into surface-averaged models using the power-law length distribution $N(L) \propto L^{-\varepsilon}$ discussed above. Various

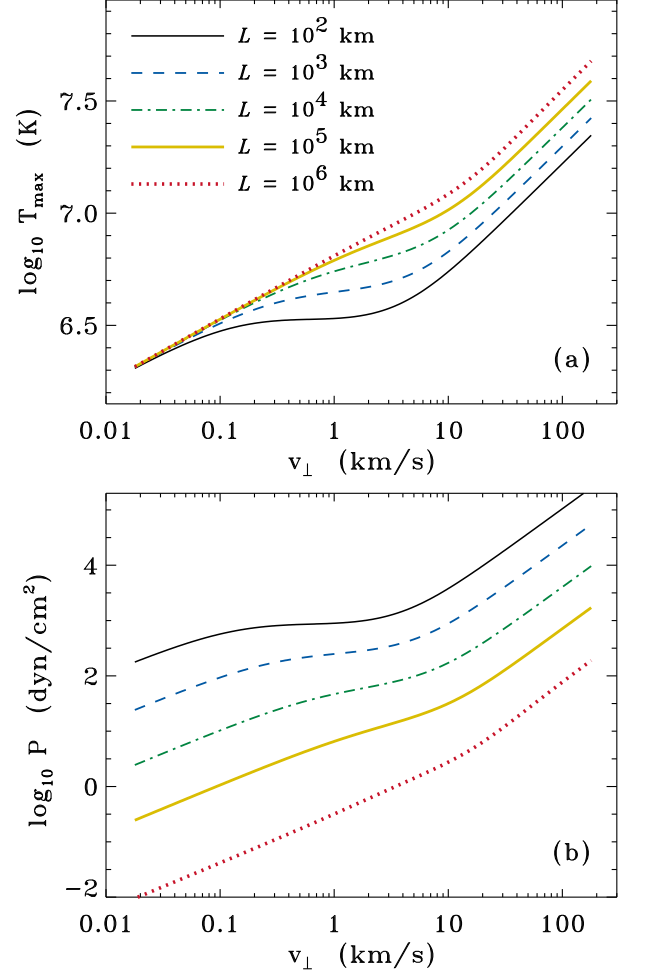


Figure 2. Dependence of (a) loop-top coronal temperature and (b) gas pressure at the coronal base on footpoint wave amplitude v_\perp (horizontal axis) and loop length L (see caption for curve identification) for our standard coronal model of AU Mic.

measurements of solar features have constrained the value of ε to be of order 2–2.5 (Aschwanden et al. 2000, 2008; Close et al. 2003), and the Cranmer (2009) study of T Tauri star X-ray emission also found that $\varepsilon \approx 2.5$ produced the most reasonable results. For completeness, we varied ε between 0 and 2.5, noting that values of the exponent greater than 2.5 produce distributions that are only marginally different from those with $\varepsilon \approx 2.5$ (i.e., once it is peaked sharply at the shortest length scales, making it even steeper does not change the resulting weighting significantly).

Figure 3(a) shows contours of L_X computed for the *ROSAT* PSPC band, and for a large grid of 250 v_\perp values by 250 ε values.² For any single value of ε , the X-ray luminosity first increases with increasing v_\perp , because the temperatures and densities in the loops are also increasing, but then L_X begins to decrease because the loops become too hot to produce significant emission in the relatively soft PSPC passband. The dotted red contour in Figure 3(a) denotes the parameters that produce agreement with the observed value of $\log L_X = 29.74$ (Hünsch et al. 1999).

² We chose not to include the smallest v_\perp amplitudes in the grid because there were no combinations of parameters in this region that produced agreement with both the X-ray and millimeter observations. The 250×250 grid encompasses the ranges $0.2 \leq v_\perp \leq 200 \text{ km s}^{-1}$ and $0 \leq \varepsilon \leq 2.5$.

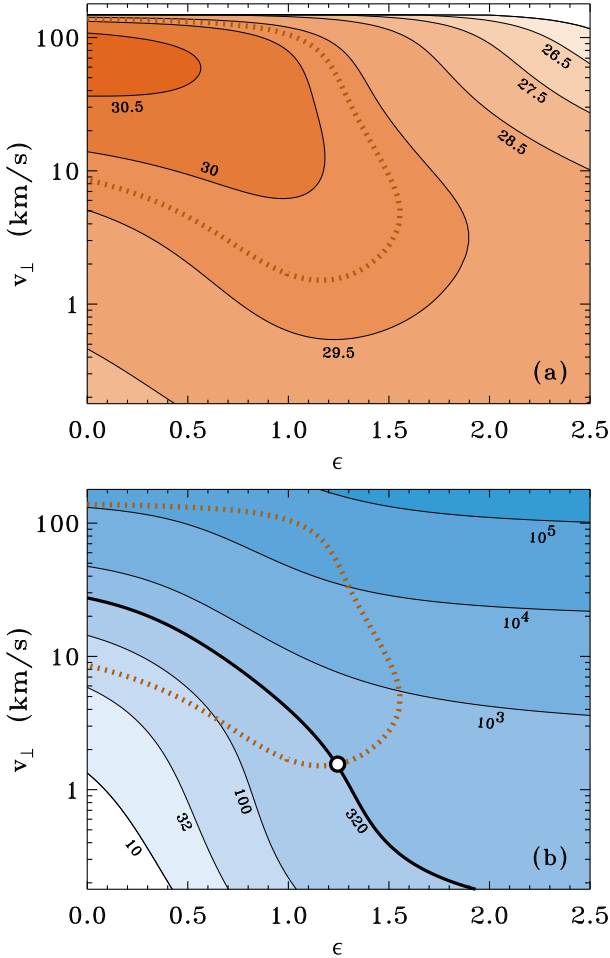


Figure 3. Synthesized observations of (a) ROSAT X-ray luminosity and (b) ALMA 1.3 mm flux for AU Mic, plotted as contours versus modeled loop length distribution exponent ϵ and surface wave velocity amplitude v_\perp . Contours are labeled with constant values of (a) $\log_{10} L_X$ (with L_X in units of erg s^{-1}), and (b) S_ν in μJy . Models agreeing with the observed value of L_X are shown in both panels with a dotted red contour, and the single model that satisfies both observational constraints is shown with a white circle.

The contours in Figure 3(b) show constant values of the free-free emission flux S_ν computed at $\lambda = 1.3$ mm. The thickest contour highlights the ALMA flux measured by MacGregor et al. (2013) for the central emission component of AU Mic. The corresponding observational contour for L_X is reproduced from Figure 3(a), and it is noteworthy that the two empirical constraints intersect one another (roughly perpendicularly) at a single parameter value. This best-fitting model has a basal velocity amplitude $v_\perp = 1.5545$ km s^{-1} and a loop distribution power-law exponent $\epsilon = 1.245$. We note also that this model has a value of v_\perp that falls within the region of likely microturbulence values (1–2 km s^{-1}) for early M-type dwarfs (Giampapa et al. 1982; Wende et al. 2009; Beeck et al. 2011).

The best-fitting model contains loops with peak temperatures between 3.7 MK (for L_{\min}) and 7.2 MK (for L_{\max}). Schneider & Schmitt (2010) produced a fit of the full *Chandra* spectrum of AU Mic with three plasma components having temperatures of 3.37, 7.78, and 17.3 MK. Our range of modeled T_{\max} values is reasonably consistent with the first two *Chandra* components. The hottest observed X-ray component may be related to intermittent nonthermal stellar flaring, which we did not include in our model.

The best-fitting model also exhibits loop-top electron densities between $7 \times 10^{11} \text{ cm}^{-3}$ (for L_{\min}) and $3 \times 10^7 \text{ cm}^{-3}$ (for L_{\max}), with the densities increasing as one goes down from the loop tops. Testa et al. (2004) found upper limits on electron densities from *Chandra* spectroscopy of AU Mic that are close to the above values. For lines of O VII and Mg XI, formed at roughly 2 MK and 7 MK respectively, Testa et al. (2004) found upper limits of 5.6×10^{11} and $5.6 \times 10^{12} \text{ cm}^{-3}$. We can also combine our model densities with the T_{\max} values given above to determine the range of gas pressures in the loops and compare them with observations. We assumed that P remained constant over the length of each loop, and the values spanned from 760 dyne cm^{-2} (for L_{\min}) to 1.8 dyne cm^{-2} (for L_{\max}). Del Zanna et al. (2002) found a best fit for the UV-derived differential emission measure of AU Mic to occur for a constant pressure of $\sim 3 \text{ dyne cm}^{-2}$, which falls inside the range of our modeled loops.

We also computed the free-free emission at longer radio wavelengths, for which there are no firm detections of AU Mic in quiescence. Both White et al. (1994) and Leto et al. (2000) gave non-detection upper limits that we can use as further tests of our model. Figure 4(a) carries over the two empirical contours from Figure 3 and also divides the parameter space into two regions: one in which the modeled emission is consistent with the White et al. (1994) upper limit for $\lambda = 2$ cm, and one in which the modeled emission exceeds that limit. Our best-fitting solution sits comfortably in the region that is consistent with all of the observed radio upper limits.

Figure 4(b) shows representative radio and millimeter spectra for a set of seven models that fall along the observational L_X contour shown in Figure 4(a). Each of these models reproduces the observed X-ray luminosity of AU Mic, but only one of them (coincidentally, the one with the lowest value of v_\perp) agrees with the ALMA flux at 1.3 mm. Four of these seven models have radio fluxes that fall below the White et al. (1994) and Leto et al. (2000) upper limits. It is noteworthy that a factor-of-two better measurement of the radio continuum at 1–10 cm would provide a much more stringent test of this model.

The shapes of the spectra in Figure 4(b) convey interesting information about the spatial variations in temperature and density. At the lowest wavelengths, the optical depth τ_ν is small (even when integrating all the way down to the coronal base), so the ν^2 dependence of the source function cancels out with the ν^{-2} in the opacity. Thus, the spectrum has a canonically flat shape that reflects only the slow wavelength dependence of the Gaunt factor. As the wavelength increases, the optical depth at the coronal base gets larger, and more of the coronal loops become optically thick. In that limit, the intensity is capped at a maximum value of

$$I_\nu \approx \frac{2k_B T \nu^2}{c^2}. \quad (11)$$

If the temperature in the emitting region was a constant, this would give a power-law spectrum going as λ^{-2} . A steepening to this shape is indeed seen around $\lambda \sim 1\text{--}5$ cm, but then it flattens out again. This is because the optical depth keeps increasing as λ increases, and the level of the $\tau_\nu = 1$ “radio photosphere” moves up from the coronal base to the tops of the loops. Because $T(s)$ increases from the base to the loop-tops, the emitting temperature to be used in Equation (11) is an increasing function of λ , too. This gives rise to an absolute value of I_ν that grows progressively larger than it would have

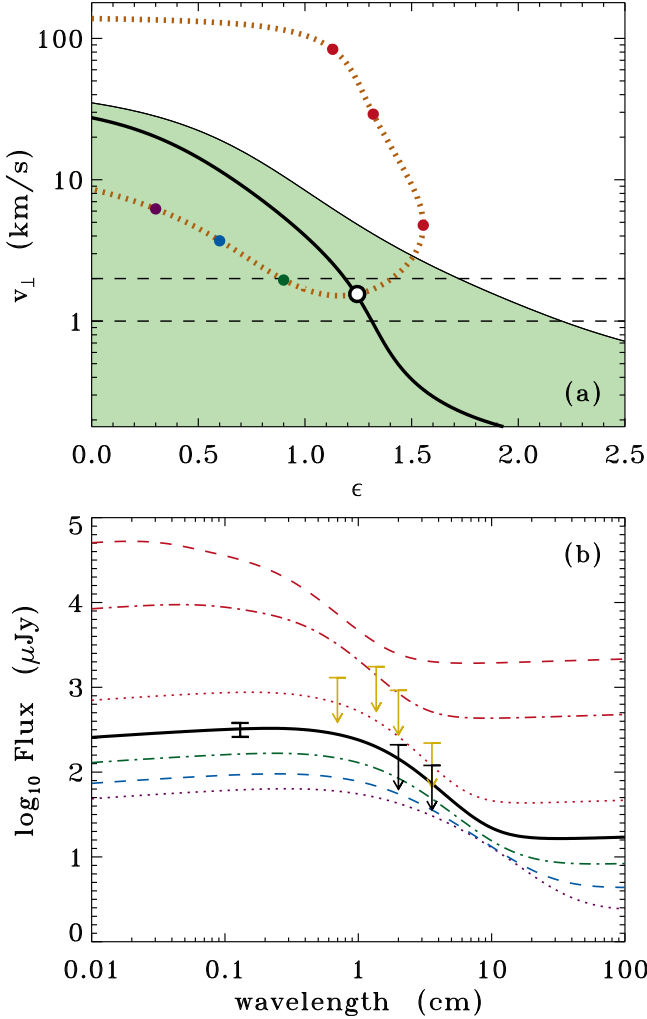


Figure 4. (a) Contours showing models that agree with observed L_X (dotted red curve) and ALMA 1.3 mm flux (thick black curve) for AU Mic, together with the region of parameter space that is consistent with the White et al. (1994) radio upper limit at $\lambda = 2$ cm (green area). Expected values of v_{\perp} from M-dwarf microturbulence are shown with thin black dashed lines. (b) Synthesized radio/mm spectra for models denoted by circles in panel (a). From bottom to top, the spectra correspond to models that follow the empirical L_X contour counterclockwise from bottom-left to top-middle in panel (a). Also shown are upper limits from White et al. (1994) (black arrows) and Leto et al. (2000) (gold arrows), and the MacGregor et al. (2013) 1.3 mm measurement (black strut).

been had the emitting temperature remained constant. Presumably as λ is increased even further, all of the loop tops will become optically thick, the emergent free-free emission will be dominated only by T_{\max} , and the spectrum will start declining again as λ^{-2} .

Lastly, we mention that the resulting values of X-ray and radio/mm emissivity do depend on the assumed value of the photospheric magnetic filling factor f_* . We ran a series of models for the standard parameter choices of $v_{\perp} = 1.5545$ km s $^{-1}$ and $\epsilon = 1.245$, where f_* was varied over two orders of magnitude from 0.01 to 1. The X-ray luminosity scales roughly as $L_X \propto f_*^{1.26}$, and the free-free emission flux at $\lambda = 1.3$ mm scales as $S_{\nu} \propto f_*^{1.39}$. These order-unity power law exponents imply that the uncertainties in the coronal loop parameters determined above may be roughly of the same magnitude as the uncertainty in our knowledge of f_* for this star.

5. DISCUSSION AND CONCLUSIONS

In this paper we began the process of exploring whether a physically motivated model of coronal loop heating could reproduce the observed properties of AU Mic. We adapted an existing model of MHD turbulent dissipation to the environment of an M1 dwarf star and treated the surface velocity amplitude v_{\perp} of stochastic Alfvénic motions as a free parameter. For a value of $v_{\perp} \approx 1.5$ km s $^{-1}$ (which is consistent with the expected granular microturbulence velocity) and a power-law probability distribution of loop lengths L that goes roughly as $L^{-1.25}$, the model successfully predicts the observed X-ray luminosity and millimeter-wave emission peak. The model is also consistent with radio upper limits measured at quiescent (non-flaring) time periods for AU Mic.

It may be possible to use independent estimates of the stellar wind mass loss rate of AU Mic to say more about the verisimilitude of the coronal heating model. Augereau & Beust (2006) determined that a mass loss rate of order $6 \times 10^{-12} M_{\odot} \text{ yr}^{-1}$ for AU Mic would generate sufficient pressure to transport dust to the outermost parts of its observed disk. We used the stellar wind model presented by Cranmer & Saar (2011) to compute how the mass loss rate of AU Mic depends on the assumed value of v_{\perp} in the treatment of coronal heating. The “default” value of $v_{\perp} = 0.02$ km s $^{-1}$ obtained from the convective turbulence model of Musielak & Ulmschneider (2002) gives rise to a mass loss rate of only $2 \times 10^{-15} M_{\odot} \text{ yr}^{-1}$. However, if we increase v_{\perp} to the empirically determined value of 1.5545 km s $^{-1}$ (see white circles in Figures 3–4), the Cranmer & Saar (2011) mass loss rate increases to $9 \times 10^{-12} M_{\odot} \text{ yr}^{-1}$. This is close to the value required by Augereau & Beust (2006) to explain the outer disk’s dust diffusion. It is at least circumstantial evidence that our loop model, “calibrated” with $v_{\perp} \approx 1.5$ km s $^{-1}$, reflects what is actually going on in the outer atmosphere of AU Mic.

Although our model accurately reproduces the magnitude of the ALMA 1.3 mm central emission peak, we do not yet have a definitive way to distinguish between this model and the idea of an inner asteroid belt proposed by MacGregor et al. (2013). For example, neither model predicts significant mid-infrared excess centered on the star, and indeed none is seen for AU Mic (Liu et al. 2004). It is possible, of course, that AU Mic has *both* an active stellar corona and a bright inner source of dusty debris. Additional information about the spectral energy distribution of the central peak resolved by ALMA would be extremely helpful to putting limits on the relative contributions of these two suggested explanations for the 1.3 mm emission. Also, better observational limits on the spatial extent of the central peak would be helpful, since the dust belt is expected to be several orders of magnitude larger in size than the source of coronal emission.

In addition to better observational constraints, there are also several ways that the models can be improved. We limited ourselves to just the time-steady component of coronal heating and not the more intermittent flaring, but the latter is known to be a non-negligible component of the total X-ray (Schneider & Schmitt 2010) and ultraviolet (Robinson et al. 2001) emission. Because we did not model flares, we also ignored the potential contributions of nonthermal electrons and gyromagnetic emission to the radio and millimeter spectra (see White et al. 1994; Linsky 1996). We did not simulate the full three-dimensional magnetic geometry of the corona of AU Mic; instead we treated its topological complexity us-

ing a simple statistical distribution of loop sizes. Future refinements to our predictions of radio, millimeter, and X-ray emission from stellar coronae should include improvements to each of the above approximations.

Finally, the success of any *ab initio* coronal model depends on our understanding of magnetic dynamos in low-mass stars. Young, rapidly rotating stars are suspected of having more vigorous convective motions and more frequent magnetic flux emergence than older stars such as the Sun (e.g., Montalbán et al. 2004; Ballot et al. 2007; Käpylä et al. 2009; Brown et al. 2011). The turbulent convection models we have used so far (Musielak & Ulmschneider 2002) do not yet include these effects, but our semi-empirical determination of $v_{\perp} \approx 1.5 \text{ km s}^{-1}$ may help put limits on how active the surfaces of young stars actually are. Still, we do not know what the granulation pattern—and the distribution of magnetic flux tubes—really looks like on the surface of a saturated-activity star. It is also possible that rapid rotation strongly affects the distribution of loop lengths (Aarnio et al. 2012). M dwarfs such as AU Mic are also close to the dividing line between having a radiative core and being fully convective. The qualitative properties of rotation, dynamos, and large-scale magnetic fields are believed to change substantially across this dividing line (Mullan & MacDonald 2001; Reiners & Basri 2007; Irwin et al. 2011; Gastine et al. 2013). These “hidden” aspects of stellar interiors may have significant impacts on the high-energy activity of a star like AU Mic and its surrounding dust and debris.

The authors gratefully acknowledge Adriaan van Ballegoijen, Nancy Brickhouse, and Hans Moritz Günther for many valuable discussions. This paper made use of the following ALMA data: ADS/JAO.ALMA#2011.0.00142.S. ALMA is a partnership of ESO (representing its member states), NSF (USA) and NINS (Japan), together with NRC (Canada) and NSC and ASIAA (Taiwan), in cooperation with the Republic of Chile. The Joint ALMA Observatory is operated by ESO, AUI/NRAO, and NAOJ. The National Radio Astronomy Observatory is a facility of the National Science Foundation operated under cooperative agreement by Associated Universities, Inc. This research made extensive use of NASA’s Astrophysics Data System and the SIMBAD database operated at CDS, Strasbourg, France. We also thank the anonymous referee for constructive suggestions that improved this paper.

REFERENCES

- Aarnio, A., Llama, J., Jardine, M., et al. 2012, *MNRAS*, 421, 1797
- Aschwanden, M. J., Lee, J. K., Gary, G. A., et al. 2008, *Sol. Phys.*, 248, 359
- Aschwanden, M. J., & Schrijver, C. J. 2002, *ApJS*, 142, 269
- Aschwanden, M. J., Tarbell, T. D., Nightingale, R. W., et al. 2000, *ApJ*, 535, 1047
- Augereau, J.-C., & Beust, H. 2006, *A&A*, 455, 987
- Ballot, J., Brun, A. S., & Turck-Chièze, S. 2007, *ApJ*, 669, 1190
- Beeck, B., Schüssler, M., & Reiners, A. 2011, in *ASP Conf. Ser.* 448, 16th Cambridge Workshop on Cool Stars, Stellar Systems, and the Sun, ed. C. Johns-Krull, M. Browning, & A. West (San Francisco, CA: ASP), 1071
- Berger, T. E., Rouppe van der Voort, L., & Löfdahl, M. 2007, *ApJ*, 661, 1272
- Berger, T. E., Schrijver, C. J., Shine, R. A., et al. 1995, *ApJ*, 454, 531
- Brown, B. P., Miesch, M. S., Browning, M. K., et al. 2011, *ApJ*, 731, 69
- Cirtain, J. W., Golub, L., Winebarger, A. R., et al. 2013, *Nature*, 493, 7433
- Close, R. M., Parnell, C. E., Mackay, D. H., & Priest, E. R. 2003, *Sol. Phys.*, 212, 251
- Cranmer, S. R. 2008, *ApJ*, 689, 316
- Cranmer, S. R. 2009, *ApJ*, 706, 824
- Cranmer, S. R. 2012, *Space Sci. Rev.*, 172, 145
- Cranmer, S. R., & Saar, S. H. 2011, *ApJ*, 741, 54
- Cranmer, S. R., & van Ballegoijen, A. A. 2005, *ApJS*, 156, 265
- Cranmer, S. R., & van Ballegoijen, A. A. 2010, *ApJ*, 720, 824
- Del Zanna, G., Landini, M., & Mason, H. E. 2002, *A&A*, 385, 968
- Dowdy, J. F., Jr., Rabin, D., & Moore, R. L. 1986, *Sol. Phys.*, 105, 35
- Dulk, G. A. 1985, *ARA&A*, 23, 169
- Feigelson, E. D., & Montmerle, T. 1999, *ARA&A*, 37, 363
- Ferguson, J. W., Alexander, D. R., Allard, F., et al. 2005, *ApJ*, 623, 585
- Gastine, T., Morin, J., Duarte, L., et al. 2013, *A&A*, 549, L5
- Giampana, M. S., Worden, S. P., & Linsky, J. L. 1982, *ApJ*, 258, 740
- Gómez, D. O., Dmitruk, P. A., & Milano, L. J. 2000, *Sol. Phys.*, 195, 299
- Güdel, M. 2002, *ARA&A*, 40, 217
- Güdel, M., & Nazé, Y. 2009, *A&A Rev.*, 17, 309
- Günther, H. M. 2013, *Astron. Nachr.*, 334, 67
- Harper, G. M., O’Riain, N., & Ayres, T. R. 2013, *MNRAS*, 428, 2064
- Hartmann, L. W., & Noyes, R. W. 1987, *ARA&A*, 25, 271
- Hebb, L., Petro, L., Ford, H. C., et al. 2007, *MNRAS*, 379, 63
- Hollweg, J. V. 1986, *J. Geophys. Res.*, 91, 4111
- Houdebine, E. R. 2009, *MNRAS*, 397, 2133
- Hünsch, M., Schmitt, J. H. M. M., Sterzik, M. F., & Voges, W. 1999, *A&AS*, 135, 319
- Irwin, J., Berta, Z. K., Burke, C. J., Charbonneau, D., Nutzman, P., West, A. A., & Falco, E. E. 2011, *ApJ*, 727, 56
- Jardine, M., & van Ballegoijen, A. A. 2005, *MNRAS*, 361, 1173
- Judge, P. G., Solomon, S. C., & Ayres, T. R. 2003, *ApJ*, 593, 534
- Kalas, P., Liu, M. C., & Matthews, B. C. 2004, *Science*, 303, 1990
- Käpylä, P. J., Korpi, M. J., & Brandenburg, A. 2009, *ApJ*, 697, 1153
- Kolmogorov, A. N. 1941, *Dokl. Akad. Nauk SSSR*, 30, 301
- Lanza, A. F. 2012, *A&A*, 544, A23
- Leto, G., Pagano, I., Linsky, J. L., Rodonò, M., & Umana, G. 2000, *A&A*, 359, 1035
- Linsky, J. L. 1996, in *ASP Conf. Ser.* 93, *Radio Emission from the Stars and the Sun*, ed. A. Taylor & J. Paredes (San Francisco, CA: ASP), 439
- Liu, M. C., Matthews, B. C., Williams, J. P., et al. 2004, *ApJ*, 608, 526
- MacGregor, M. A., Wilner, D. J., Rosenfeld, K. A., et al. 2013, *ApJ*, 762, L21
- Magic, Z., Collet, R., Asplund, M., et al. 2013, *A&A*, submitted, arXiv:1302.2621
- Martens, P. C. H. 2010, *ApJ*, 714, 1290
- McKee, C. F., & Ostriker, E. C. 2007, *ARA&A*, 45, 565
- Montalbán, J., D’Antona, F., Kupka, F., & Heiter, U. 2004, *A&A*, 416, 1081
- Mullan, D. J., & MacDonald, J. 2001, *ApJ*, 559, 353
- Musielak, Z. E. 2004, in *IAU Symp.* 219, *Stars as Suns: Activity, Evolution, and Planets*, ed. A. Dupree & A. Benz (San Francisco, CA: ASP), 437
- Musielak, Z. E., & Ulmschneider, P. 2002, *A&A*, 386, 606
- Parker, E. N. 1972, *ApJ*, 174, 499
- Rappazzo, A. F., Velli, M., Einaudi, G., & Dahlburg, R. B. 2008, *ApJ*, 677, 1348
- Reiners, A., & Basri, G. 2007, *ApJ*, 656, 1121
- Robinson, F. J., Demarque, P., Li, L. H., et al. 2004, *MNRAS*, 347, 1208
- Robinson, R. D., Linsky, J. L., Woodgate, B. E., et al. 2001, *ApJ*, 554, 368
- Rosner, R., Tucker, W. H., & Vaiana, G. S. 1978, *ApJ*, 220, 643
- Saar, S. H. 2001, in *ASP Conf. Ser.* 223, *11th Cambridge Workshop on Cool Stars, Stellar Systems, and the Sun*, ed. R. Garcia Lopez, R. Rebolo, & M. Zapaterio Osorio (San Francisco, CA: ASP), 292
- Schneider, P. C., & Schmitt, J. H. M. M. 2010, *A&A*, 516, A8
- Schrijver, C. J., & Harvey, K. L. 1989, *ApJ*, 343, 481
- Schrijver, C. J., Sandman, A. W., Aschwanden, M. J., et al. 2004, *ApJ*, 615, 512
- Stelzer, B., Marino, A., Micela, G., et al. 2013, *MNRAS*, 431, 2063
- Strubbe, L. E., & Chiang, E. I. 2006, *ApJ*, 648, 652
- Testa, P., Drake, J. J., & Peres, G. 2004, *ApJ*, 617, 508
- van Ballegoijen, A. A. 1986, *ApJ*, 311, 1001
- van Ballegoijen, A. A., Asgari-Targhi, M., Cranmer, S. R., & DeLuca, E. 2011, *ApJ*, 736, 3
- van Leeuwen, F. 2007, *A&A*, 474, 653
- Wende, S., Reiners, A., & Ludwig, H.-G. 2009, in *AIP Conf. Proc.* 1094, *15th Cambridge Workshop on Cool Stars, Stellar Systems, and the Sun*, ed. E. Stempels (Melville, NY: AIP), 816
- White, S. M., Lim, J., & Kundu, M. R. 1994, *ApJ*, 422, 293
- Wiegmann, T., & Sakurai, T. 2012, *Living Rev. Solar Phys.*, 9, 5
- Wilner, D. J., Andrews, S. M., MacGregor, M. A., & Hughes, A. M. 2012, *ApJ*, 749, L27
- Wright, N. J., Drake, J. J., Mamajek, E. E., & Henry, G. W. 2011, *ApJ*, 743, 48